Liver Fat Droplet Dependency on Ultrasound Backscatter Coefficient in Nonalcoholic Fatty Liver

Yashuo Wu
Bioacoustics Research Laboratory, Department of Electrical and Computer Engineering
University of Illinois at Urbana-Champaign
Urbana, US
yashuow2@illinois.edu

Leonardo Lopez
Bioacoustics Research Laboratory, Department of Electrical and Computer Engineering
University of Illinois at Urbana-Champaign
Urbana, US
ll10@illinois.edu

Michael P. Andre
Department of Radiology
University of California, San Diego
La Jolla, US
mandre@ucsd.edu

Rohit Loomba
NAFLD Research Center, Division of Gastroenterology, Department of Medicine
University of California, San Diego
La Jolla, US
roloomba@ucsd.edu

Claude B. Sirlin
NAFLD Research Center, Division of Gastroenterology, Department of Medicine
University of California, San Diego
La Jolla, US
csirlin@health.ucsd.edu

Mark A. Valasek
Department of Pathology
University of California, San Diego
La Jolla, US
mvalasek@ucsd.edu

Matthew A. Wallig
Department of Pathobiology
University of Illinois at Urbana-Champaign
Urbana, US
mawallig@illinois.edu

William D. O'Brien, Jr.
Bioacoustics Research Laboratory, Department of Electrical and Computer Engineering
University of Illinois at Urbana-Champaign
Urbana, US
wdo@uiuc.edu

Aiguo Han
Bioacoustics Research Laboratory, Department of Electrical and Computer Engineering
University of Illinois at Urbana-Champaign
Urbana, US
han51@illinois.edu

***Abstract*—Quantitative ultrasound (QUS) techniques are diagnostically useful in assessing nonalcoholic fatty liver disease (NAFLD). From previous studies, the backscatter coefficient (BSC) correlates with liver fat fraction, but the mechanisms have not been determined. Understanding the ultrasound scattering mechanisms will lead to better acoustic scattering models and more accurate diagnostics. The purpose of this study is to test the following hypothesis: Fat droplet deposition in hepatocytes alters the locations of hepatocyte nuclei, changing the spatial distribution of the nuclei, which leads to the change in the structure function (SF), a factor of the BSC. The SF, determined by the distribution of the nuclei, is correlated with the fat fraction. To test this hypothesis, hematoxylin and eosin-stained liver histopathological slides from 48 participants were digitized (40×). One to 5 regions (453.6 μm × 453.6 μm) were selected from each participant's slide(s), yielding 218 images in total. For each image, hepatocyte nuclei and fat droplets each were automatically recognized. SF versus frequency was calculated from the nuclear distribution. Liver fat fraction was determined from the fractional surface area of fat droplets. SF was positively correlated with the liver fat fraction (Pearson's $r \sim 0.4$, $p < 10^{-4}$) below 30 MHz (including clinically relevant frequencies 3 - 5 MHz). In conclusion, this study shows the fat droplets change the distribution of hepatocyte nuclei, which is a factor contributing to the correlation between fat fraction and BSC.**

Keywords—structure function, acoustic scattering, histology, nuclei recognition, quantitative ultrasound

I. Introduction

Quantitative imaging is playing an increasingly important role in medical diagnosis. Quantitative ultrasound (QUS), the extraction of quantitative parameters from ultrasound backscattered signals, has promising clinical applications in tissue characterization and disease diagnosis [1]. Among other successes, recent human studies have demonstrated the capabilities of spectral-based QUS techniques in quantifying liver steatosis [2-4]. The QUS attenuation coefficient (AC) and backscatter coefficient (BSC) have been shown to be significantly correlated to the fat content in the liver.

While the positive correlation between liver fat content and QUS parameters has been established in human studies, the causal relationship has not been elucidated. A clear understanding of the mechanisms by which liver fat droplet deposition causes changes in the QUS parameters will guide the proper use of the QUS techniques and also lead to further improvement of the techniques.

The purpose of this study is to investigate how liver fat droplets change the BSC, a fundamental QUS parameter, by using digitized hematoxylin and eosin (H&E)-stained histopathological liver slides. We have hypothesized two independent mechanisms. 1) Fat droplets constitute acoustic scatterers in the liver, causing more scattering and increasing the BSC. 2) Hepatocyte nuclei are also acoustic scatterers. Fat droplet deposition in hepatocytes alters the locations of the

hepatocyte nuclei within the hepatocytes, which changes the spatial distribution of the nuclei. The BSC is influenced by the spatial distribution of scatterers according to acoustic scattering theories. The effect of the scatterer spatial distribution on the BSC is quantified by the structure function (SF) as a factor of the BSC. Therefore, fat droplet deposition changes the hepatocyte nuclear distribution, which changes the SF and hence the BSC. Due to space limit, this study focuses on the second mechanism, i.e., fat droplets change the SF.

II. Structure Function Theory

The concept of the SF was originally developed in statistical mechanics, first applied to acoustic scattering by Twersky [5,6], and first used to describe biological scatterers by Fontaine et al. [7]. The SF has been shown to play a role in the ultrasound scattering of a wide variety of materials [8-15]. The SF theory is briefly introduced as follows.

Consider a plane wave incident on a scattering volume that contains N discrete scatterers. The differential scattering cross section per unit volume, σ_d, observed in the far field, can be expressed as [13, 16]

$$\sigma_d(\mathbf{K}) = \frac{1}{V}\left|\sum_{j=1}^{N} \Phi_j(\mathbf{K}) e^{i\mathbf{K}\cdot\mathbf{r}_j}\right|^2, \quad (1)$$

where $\mathbf{r}_j$ is the position of the jth scatterer, $\Phi_j(\mathbf{K})$ is the complex scattering amplitude of the jth scatterer and $\mathbf{K}$ is the scattering vector, whose magnitude is given by $|\mathbf{K}| = 2k\sin(\theta/2)$, where θ is the scattering angle, and k is the wavenumber. If the scatterers are spatially uncorrelated and N is large, the scattering is incoherent and the expected differential cross section per unit volume becomes

$$\sigma_{d,incoherent} = \frac{1}{V}\sum_{j=1}^{N}\left|\Phi_j(\mathbf{K})\right|^2. \quad (2)$$

The SF is defined as

$$S(\mathbf{K}) = \frac{\sigma_d(\mathbf{K})}{\sigma_{d,incoherent}(\mathbf{K})}. \quad (3)$$

Assuming the complex scattering amplitudes $\Phi_j(\mathbf{K})$ are identical for all scatterers, (3) may be simplified as

$$S(\mathbf{K}) = \frac{1}{N}\left|\sum_{j=1}^{N} e^{-i\mathbf{K}\cdot\mathbf{r}_j}\right|^2, \quad (4)$$

which is used to determine the SF from histology (III-B).

III. Methodology

A. Automatic Nuclei Recognition

The H&E-stained liver slides of 48 participants with and without nonalcoholic fatty liver disease (NAFLD) were digitized using a Leica AT2 scanner at 40× apparent magnification. One to 5 regions of interest (ROIs) were chosen from each slide, and 218 ROIs were obtained in total. Each ROI had a size of 453.6 μm × 453.6 μm, with a resolution of 3.97 pixels/μm. Fig. 1(a) is an example ROI.

A series of operations were developed to automatically recognize hepatocyte nuclei. First, the k-means (k = 4) clustering technique was used to classify the pixels based on color into four categories: white, light pink, pink, and blue. Blue was considered to represent the nuclei and other colors were considered the background. A binary image consisting of the nuclei and the background was generated.

Afterward, a series of morphological operations were applied to the resulting binary images to improve the nuclei recognition results. Specifically, opening was used to remove objects much smaller than typical hepatocyte nuclei. Closing was applied to fill in holes in the regions of nuclei. Erosion was applied to separate the boundaries of multiple nuclei in a cluster while dilation was used to extend the boundary.

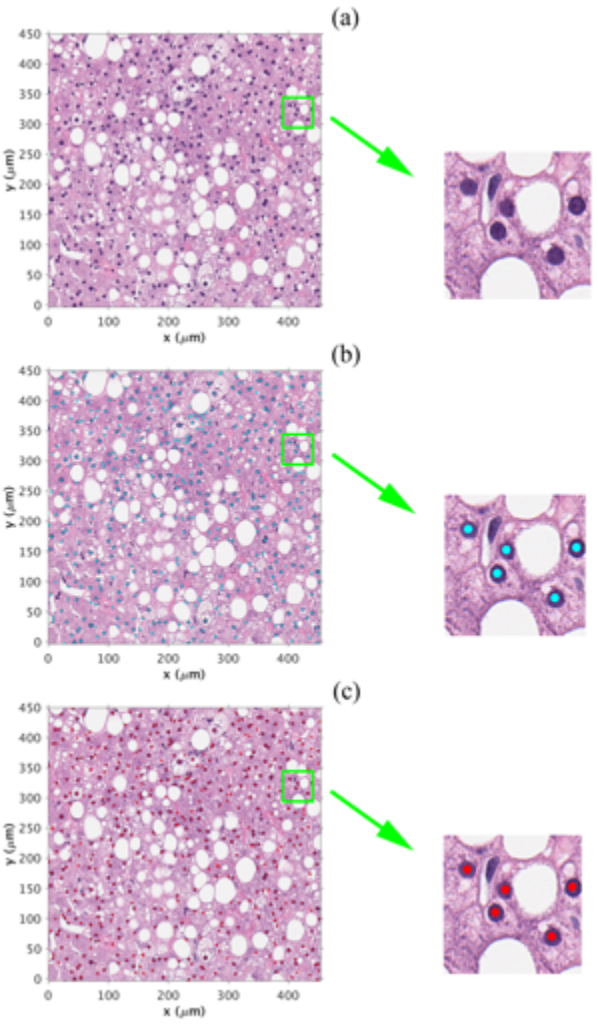

Fig. 1 (a) An ROI of an original H&E image and zoomed-in view of the region indicated by the green box. The white regions are fat droplets. (b) An ROI superimposed with automatically recognized nuclei (in cyan). (c) An ROI superimposed with manually recognized nuclei (in red). Note that the lymphocyte in the zoomed-in view of (b) and (c) was not recognized as hepatocyte nuclei.

Finally, objects whose eccentricity was larger than 0.8 were removed. This step removed lymphocytes and other particles that were not hepatocyte nuclei (Fig. 1(b)).

B. *Structure Function Calculation from Histology*

The SF was calculated by using the 2-D version of (4) and the automatically recognized nuclear centers. Specifically, the vector **K** was chosen as $\mathbf{K} = \frac{2\pi}{L}(n_x\hat{x} + n_y\hat{y})$, where $n_x, n_y, = \pm 1, \pm 2, ...$, and L is the side length of the ROI. The magnitude of **K** was then determined by $k = \frac{2\pi}{L}\sqrt{n_x^2 + n_y^2}$. Circular averaging was performed with a resolution of $\frac{2\pi}{L}$ for k. For backscattering, frequency was determined by $f = kc/4\pi$, where the speed of sound c = 1540 m/s. The frequency range used to calculate the SF was 3.4 to 40 MHz. The low frequency limit was determined by the ROI size [14, 15] and the upper frequency was extended beyond conventional clinical frequency ranges to provide theoretical insights.

C. *Manual Nuclei Recognition*

Manual recognition of hepatocyte nuclei was performed to evaluate the accuracy of automatic recognition (III-B) for purposes of SF calculation. Manual nuclei recognition (Fig. 1(c)) was performed in a subset of ROIs (n=29). The SF versus frequency curves calculated based on the automatic and manual recognition were compared. The agreement was evaluated by the R^2 value.

D. *Fat Fraction Determination Using Histology*

Fat droplets were recognized automatically to calculate fat fraction for each ROI. The fat fraction was calculated by the ratio of the area occupied by all fat droplets to the area of the ROI. Fat droplets were recognized based on their color, shape, and size. Specifically, fat droplets appeared to be white in all ROIs. The circularity of fat droplets was between 0.25 to 1.2. The size of a fat droplet was larger than the average size of a nucleus (radius = 3 μm). Those characteristics were used to determine the threshold for color, circularity, and size in fat droplet recognition.

E. *Correlation between Fat Fraction and SF*

Pearson correlation coefficient was used to evaluate the correlation between the fat fraction estimated in III-D and the SF at each frequency obtained in III-B.

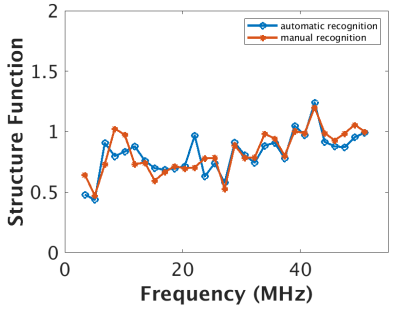

Fig. 2 Comparison between SF versus frequency curves obtained from automatically recognized nuclei and manually recognized nuclei for the same ROI.

IV. Results and Discussion

The SF calculated from the automatically recognized nuclei showed good agreement with the SF calculated from the manually recognized nuclei, with an average R^2 value of 0.63. Fig. 2 is an example of the comparison between the SF curves calculated automatically recognized and manually recognized nuclei. The two SF curves showed similar trends. The R^2 value was 0.62 in this case. These results justified the use of automatic nuclei recognition for SF calculation.

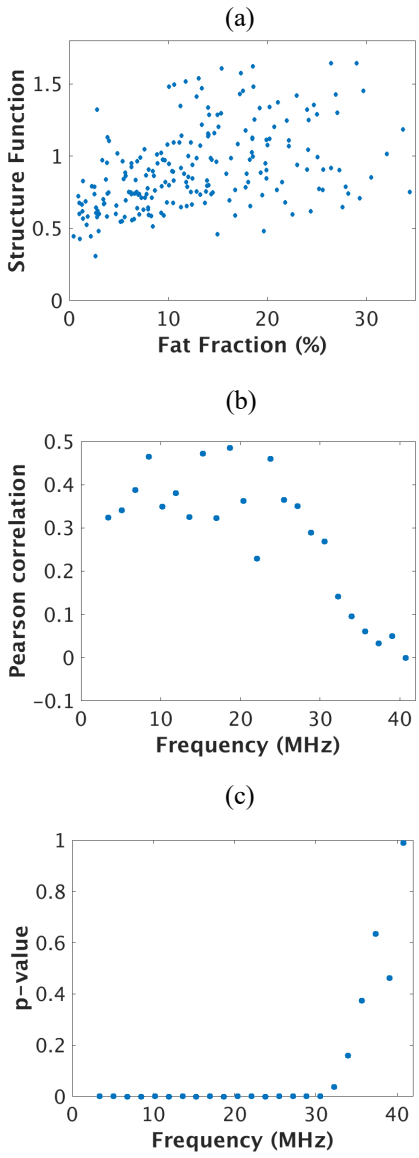

Fig 3. (a) Scatter plot of average SF between 3.4 and 5.1 MHz versus fat fraction. (b) Pearson correlation coefficient between fat fraction and SF at each frequency within 3.4 – 40 MHz. (c) Corresponding p-values of the Pearson correlation analysis.

The average SF between 3.4 and 5.1 MHz versus fat fraction is shown in Fig. 3(a), where each point represents one ROI. The SF was positively correlated with the fat fraction (Pearson correlation coefficient r = 0.43 and $p < 10^{-4}$. The fat

fraction ranged between close to 0 and 35%. The SF ranged between 0.3 and 1.6. The SF deviated from unity, suggesting the non-random spatial distribution of hepatocyte nuclei.

Pearson correlation coefficient values and the corresponding p-values were plotted in Fig. 3(b) and Fig. 3(c), respectively, for each frequency between 3.4 and 40 MHz. The correlation coefficient values fluctuated around 0.4 at frequencies lower than 30 MHz, and the corresponding p-values were far lower than 0.01, indicating that the correlation between SF and fat fraction was significant in all frequencies below 30 MHz.

The statistically significant positive correlation between SF and fat fraction suggested that the fat droplet deposition altered the nuclei spatial distribution and the SF, which in part explained the observed positive correlation between fat fraction and BSC in the literature. Also, the positive correlation between SF and fat fraction suggested the potential of developing the SF as an independent biomarker for liver fat quantification.

V. Conclusion

This study supports the hypothesis that the fat droplets change the spatial distribution of the hepatocyte nuclei and lead to changes in the structure function, which partially explains the positive correlation between BSC and fat fraction, and demonstrates the usefulness of the SF in understanding ultrasonic scattering in human liver.

Acknowledgment

This study was supported by the National Institutes of Health under award numbers R01DK106419 and R01CA226528. The content is solely the responsibility of the authors and does not necessarily represent the official views of the National Institutes of Health.

References

[1] M. L. Oelze and J. Mamou, "Review of quantitative ultrasound: Envelope statistics and backscatter coefficient imaging and contributions to diagnostic ultrasound," *IEEE Trans. Ultrason. Ferroelectr. Freq. Control,* vol. 63, no. 2, pp. 336–351, 2016.

[2] S. C. Lin, E. Heba, T. Wolfson, B. Ang, A. Gamst, A. Han, J. W. Erdman, Jr., W. D. O'Brien, Jr., M. P. Andre, C. B. Sirlin, and R. Loomba, "Noninvasive diagnosis of nonalcoholic fatty liver disease and quantification of liver fat using a new quantitative ultrasound technique," *Clin. Gastroenterol. Hepatol.*, vol. 13, no. 7, pp. 1337–1345, 2015.

[3] J. S. Paige, G. S. Bernstein, E. Heba, E. A. C. Costa, M. Fereirra, T. Wolfson, A. C. Gamst, M. A. Valasek, G. Y. Lin, A. Han, J. W. Erdman, Jr., W. D. O'Brien, Jr., M. P. Andre, R. Loomba, and C. B. Sirlin, "A pilot comparative study of quantitative ultrasound, conventional ultrasound, and MRI for predicting histology-determined steatosis grade in adult nonalcoholic fatty liver disease," *Am. J. Roentgenol*., vol. 208, no. 5, pp. W168–W177, 2017.

[4] A. Han, Y. N. Zhang, A. S. Boehringer, V. Montes, M. P. Andre, J. W. Erdman, Jr., R. Loomba, M. A. Valasek, C. B. Sirlin, and W. D. O'Brien, Jr., "Assessment of hepatic steatosis in nonalcoholic fatty liver disease using quantitative ultrasound," *Radiology*, vol. 295, no. 1, pp. 106–113, 2020.

[5] V. Twersky, "Low-frequency scattering by correlated distributions of randomly oriented particles," *J. Acoust. Soc. Amer.*, vol. 81, no. 5, pp. 1609–1618, 1987.

[6] V. Twersky, "Low-frequency scattering by mixtures of correlated nonspherical particles," *J. Acoust. Soc. Amer*., vol. 84, no. 1, pp. 409–415, 1988.

[7] I. Fontaine, M. Bertrand, and G. Cloutier, "A system-based approach to modeling the ultrasound signal backscattered by red blood cells," *Biophys. J.*, vol. 77, no. 5, pp. 2387–2399, Nov. 1999.

[8] D. Savéry and G. Cloutier, "A point process approach to assess the frequency dependence of ultrasound backscattering by aggregating red blood cells," *J. Acoust. Soc. Amer.*, vol. 110, no. 6, pp. 3252–3262, 2001.

[9] J. W. Hunt, A. E. Worthington, A. Xuan, M. C. Kolios, G. J. Czarnota, and M. D. Sherar, "A model based upon pseudo regular spacing of cells combined with the randomisation of the nuclei can explain the significant changes in high-frequency ultrasound signals during apoptosis," *Ultrasound Med. Biol.*, vol. 28, no. 2, pp. 217–226, 2002.

[10] E. Franceschini and R. Guillermin, "Experimental assessment of four ultrasound scattering models for characterizing concentrated tissue-mimicking phantoms," *J. Acoust. Soc. Amer.*, vol. 132, no. 6, pp. 3735–3747, 2012.

[11] A. Han and W. D. O'Brien, Jr., "Structure function for highconcentration biophantoms of polydisperse scatterer sizes," *IEEE Trans. Ultrason., Ferroelect., Freq. Control*, vol. 62, no. 2, pp. 303–318, 2015.

[12] P. Muleki-Seya et al., "High-frequency quantitative ultrasound spectroscopy of excised canine livers and mouse tumors using the structure factor model," *IEEE Trans. Ultrason., Ferroelect., Freq. Control*, vol. 63, no. 9, pp. 1335–1350, 2016.

[13] A. Han and W. D. O'Brien, Jr., "Structure function estimated from histological tissue sections," *IEEE Trans. Ultrason., Ferroelect., Freq. Control*, vol. 63, no. 9, pp. 1296–1305, 2016.

[14] A. Han. "A method for stereological determination of the structure function from histological sections of isotropic scattering media," *IEEE Trans. Ultrason., Ferroelect., Freq. Control*, vol. 65, no. 6, pp. 1007–1016, 2018.

[15] A. C. Luchies and M. L. Oelze, "Effects of the container on structure function with impedance map analysis of dense scattering media," *J. Acoust. Soc. Amer.*, vol. 143, no. 4, pp. 2172–2181, 2018.

[16] M. F. Insana, R. F. Wagner, D. G. Brown, and T. J. Hall, "Describing small-scale structure in random media using pulse-echo ultrasound," *J. Acoust. Soc. Amer*., vol. 87, no. 1, pp. 179–192, 1990.